KSCE Journal of Civil Engineering (2016) 20(5):1958-1965
DOI 10.1007/s12205-015-0057-1

Structural Engineering
pISSN 1226-7988, eISSN 1976-3808
www.springer.com/12205

Semi-empirical and Efficient Solutions for FGPM Hollow Spheres in Hygrothermal Environment

M. N. M. Allam*, R. Tantawy, and A. M. Zenkour*****

Received January 19, 2015/Accepted August 28, 2015/Published Online November 23, 2015

Abstract

This paper presents semi-analytical solutions for functionally graded piezoelectric hollow spheres. The hollow sphere is subjected to pressure on the boundary surface, electric potentials difference between the outer and inner surfaces, and uniform distribution of hygrothermal effect. It is assumed that the material properties of the sphere are graded in the radial direction according to a power law distribution of the volume fraction of the constituents. Some cases of boundary conditions are presented for stresses, electric potentials and displacement. Finally, numerical results for radial displacement, electric potential and stresses are carried out and discussed. The effects of different parameters are investigated. It can be concluded that the gradient of the material properties have particular influence in modern engineering design.

Keywords: *piezoelectric, functionally graded, hygrothermal effect, semi-analytical solution*

1. Introduction

Material properties in Functionally Graded Material (FGM) structures are changed through the thickness distribution by using power or exponential law of the volume fraction of the constituents. The Functionally Graded Piezoelectric Material (FGPM) is considered as one kind of piezoelectric material with properties varying continuously in the radial or the thickness direction. FGPMs are composite materials intentionally designed to have desirable properties for specific applications. The advantage of these new types of materials is that they can improve the reliability or the life of piezoelectric devices.

There have been some studies concerned with thermal stresses or piezoelectric effect in the basic structural components of FGMs. Ootao and Tanigawa (2007) have presented the theoretical treatment due to uniform heat supply of transient piezo-thermo-elastic problem of FG hollow spheres. They analyzed the transient 1-D temperature by the method of Laplace transformation. Dai *et al.* (2007) have presented analytical studies on electro-magneto-elastic behaviors of FGPM structures. These solid structures are placed in a uniform magnetic field and subjected to external pressures and electric loadings. Dai *et al.* (2010b) have presented the analytical solution for piezoelectric behaviors of FGPM hollow spherical and cylindrical structures. Allam and Tantawy (2011) have presented an analytical solution for the interaction of different field quantities of hollow structures made of viscoelastic isotropic material, reinforced with elastic isotropic fibers. Loghman *et al.* (2012) have investigated the magnetothermoelastic creep behaviour of thick-walled FGM spheres. Dai *et al.* (2012) have presented an analytical solution for time-dependent behaviours of a FGPM hollow sphere under the coupling of multi-fields.

The mechanical properties of FGMs are often represented in two ways: one of them is the exponentially graded forms (Zenkour, 2007; 2008) and the other is the power law variations (Reddy and Chin, 1998; Reddy, 2000; Reddy and Cheng, 2001; Zenkour, 2005a, b; Zenkour, 2006a). Reddy and Chin (1998) have presented the thermoelastic responses of FG cylinders and plates. Reddy and Cheng (2001) have used an asymptotic method to treat the 3-D thermomechanical analysis of simply-supported, FG rectangular plates.

The hygrothermal stress analyses of different plate structures have been the subject of research interest of many investigators (Whiteny and Ashton, 1971; Patel *et al.*, 2002; Bahrami and Nasier, 2007; Lo *et al.*, 2010; Zenkour, 2012a, b). In this paper, the hygrothermal analyses of FGPM hollow spheres are presented. The displacement, stresses and electric potentials are obtained via a semi analytical solution technique for the electro-thermo-hygro-mechanical problem.

2. Basic Equations of the Problem

Let us consider a hollow sphere, having perfect conductivity.

*Professor, Dept. of Mathematics, Faculty of Science, Mansoura University, Mansoura 35516, Egypt (E-mail: mallam@mans.edu.eg)
**Assistant Professor, Dept. of Mathematics, Faculty of Science, Damietta University, Damietta 34517, Egypt (E-mail: rania_eltantwy@yahoo.com)
***Professor, Dept. of Mathematics, Faculty of Science, King Abdulaziz University, P.O. Box 80203, Jeddah 21589, Saudi Arabia; Dept. of Mathematics, Faculty of Science, Kafrelsheikh University, Kafr El-Sheikh 33516, Egypt (Corresponding Author, E-mail: zenkour@sci.kfs.edu.eg)

The spherical coordinate of any representative point (r, θ, φ) is considered. The FGM hollow sphere is subjected to rapid change in temperature $T(r)$ and moisture concentration $C(r)$. The variation of material property $P(r)$ along the radial direction of the FG sphere is assumed to be of the following form (Zenkour 2006b):

$$P(r) = (p^b - p^a)\left(\frac{r-a}{b-a}\right)^n + p^a \tag{1}$$

where p^a and p^b are the corresponding properties of the inner and outer surfaces of the sphere, a and b are the inner and outer radii of the sphere, $n \geq 0$ is the volume fraction exponent or the grading index.

For the axisymmetric plane strain assumption, the field quantities such as displacement, stresses, electric potential and electric displacement may be expressed by $u(r)$, $\sigma_i(r), (r = r, \theta)$, $\psi(r)$ and $D_r(r)$, respectively. The constitutive equations are given by (Sinha, 1962; Raja *et al.*, 2004; Dai and Wang, 2005):

$$\begin{Bmatrix} \sigma_r \\ \sigma_\theta \end{Bmatrix} = \begin{bmatrix} c_{rr} & 2c_{r\theta} & e_{rr} \\ c_r\theta & c_{\theta\varphi} + c_{\theta\theta} & e_{r\theta} \end{bmatrix} \begin{Bmatrix} \frac{du}{dr} \\ \frac{u}{r} \\ \frac{d\psi}{dr} \end{Bmatrix} - \begin{Bmatrix} \lambda_r \\ \lambda_\theta \end{Bmatrix} T(r) - \begin{Bmatrix} \eta_r \\ \eta_\theta \end{Bmatrix} C(r) \tag{2}$$

and

$$D_r = e_{rr}\frac{du}{dr} + 2e_{r\theta}\frac{u}{r} - \varepsilon_{rr}\frac{d\psi}{dr} + p_{11}T(r) \tag{3}$$

where $c_{ij}(i = r, \theta, j = r, \theta, \varphi)$, $e_{rj}(j = r, \theta)$, ε_{rr} and p_{11} are elastic coefficients, piezoelectric parameters, dielectric parameters and pyroelectric coefficients, respectively. In addition, $\eta_i(i = r, \theta)$ are the coefficients of moisture expansion, while λ_i represent the stress-temperature moduli that take the form:

$$\begin{Bmatrix} \lambda_r \\ \lambda_\theta \end{Bmatrix} = \begin{bmatrix} c_{rr} & 2c_{r\theta} \\ c_{r\theta} & c_{\theta\varphi} + c_{\theta\theta} \end{bmatrix} \begin{Bmatrix} \alpha_r \\ \alpha_\theta \end{Bmatrix} \tag{4}$$

in which α_i are the thermal expansion coefficients. Generally, this study assumes that $c_{ij}(i = r, \theta, j = r, \theta, \varphi)$, $e_{rj}(j = r, \theta)$, ε_{rr}, $\eta_r(i = r, \theta)$, and p_{11} of the FG sphere change continuously through its radial direction and obey the gradation relation given in Eq. (1).

The temperature distribution through the radial direction of the sphere is governed by the heat conduction equation

$$k\nabla^2 T(r) + q(r) = 0 \tag{5}$$

where $\nabla^2 = \frac{d^2}{dr^2} + \frac{1}{r}\frac{d}{dr}$, k is the mean of thermal conductivity and $q(r)$ is the heat generation function.

In modeling, the transient moisture diffusion equation may appear in the same manner as that of the transient heat conduction equation. It is described with aid of the Fick's law as:

$$\nabla^2 C(r) = 0 \tag{6}$$

The equilibrium equation of the FG sphere without the influence of the body forces is presented as:

$$\frac{d\sigma_r}{dr} + \frac{2(\sigma_r - \sigma_\theta)}{r} = 0 \tag{7}$$

In addition, the charge equation of electrostatics in the absence of free charge density is expressed as (Heyliger, 1997):

$$\frac{dD_r}{dr} + \frac{2D_r}{r} = 0 \tag{8}$$

3. Elastic Solution for the FGPM Sphere

The elastic solutions for the FGPM hollow sphere are given by solving the temperature, moisture, and equilibrium equations. All resulting constants can be solved by the application of the mechanical, electric, and boundary conditions.

The temperature is generated at a position-dependent rate within the inner surface of the present FGP hollow sphere and it is transferred to the outer insulated surface. So, the temperature boundary conditions are given by:

$$T(r)\big|_{r=a} = T_0, \ \left.\frac{dT(r)}{dr}\right|_{r=b} = 0 \tag{9}$$

where T_0 is the reference initial temperature. The internal energy generation within the inner and outer surfaces is described by the heat generating function

$$q(r) = -\frac{Q}{ab}(r-a)(r-a), \ a \leq r \leq b \tag{10}$$

where Q denotes the constant rate of internal energy generation. So, the general solution of the heat conduction equation given in Eq. (5) is

$$T(r) = \frac{Qr^2}{144kab}[9(r^2 + 4ab) - 16r(a+b)] + c_1 \ln(r) + c_2 \tag{11}$$

where c_1 and c_2 are arbitrary constants. They can be determined from the boundary conditions given in Eq. (9) in the form:

$$\left.\begin{aligned} c_1 &= \frac{Qb^2}{12ka}(b-2a) \\ c_2 &= \frac{Q}{144kab}[a^3(7a-20b) - 12b^3\ln(a)(b-2a)] + T_0 \end{aligned}\right\} \tag{12}$$

The dimensionless temperature T/T_0 is plotted in Fig. 1(a) through the radial direction; where the constant rate of internal energy generation Q and the thermal conductivity k are given, respectively, by

$$Q = 12(Wm^{-3}), \kappa = 0.35(WK^{-1}m^{-1}) \tag{13}$$

In addition, the inner and outer radii of the FGPM sphere are chose arbitrarily as $a = 0.2$ m and $b = 1$ m.

Also the general solution of Eq. (6) is

$$C(r) = c_3 ln(r) + c_4 \tag{14}$$

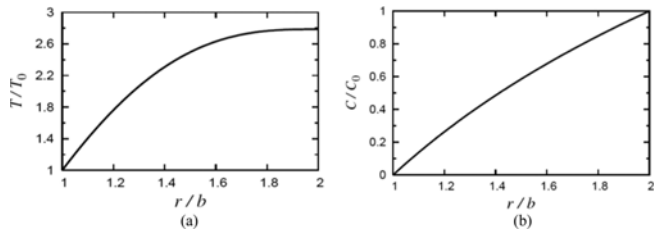

Fig. 1. Hygrothermal Distribution in the FGPM Hollow Sphere: (a) Temperature Distribution, (b) Moisture Distribution

where c_3 and c_4 are arbitrary integration constants. The boundary conditions for the moisture concentration are

$$C(r)|_{r=a}=0,\quad C(r)|_{r=b}=C_0 \tag{15}$$

where C_0 is the reference initial moisture concentration. Then, the constants c_3 and c_4 are given by

$$c_3=\frac{c_o}{ln(b)-ln(a)},\qquad c_4=-\frac{c_o ln(a)}{ln(b)-ln(a)} \tag{16}$$

Figure 1(b) shows the distribution of the dimensionless moisture concentration C/C_0 through the radial direction.

In addition, the solution of the charge equation of electrostatics is given by

$$D_r=\frac{A_1}{r^2} \tag{17}$$

where A_1 is an unknown constant. Thus, Eqs. (3) and (17) with the aid of the gradation relation given in Eq. (1), yield

$$\frac{d\psi}{dr}=\frac{1}{\varepsilon_{rr}}\left(e_{rr}\frac{du}{dr}+2e_{r\theta}\frac{u}{r}+p_{11}T(r)-\frac{A_1}{r^2}\right) \tag{18}$$

The radial and circumference stresses given in Eq. (2) with the aid of Eqs. (1) and (18) can be summarized as

$$\begin{Bmatrix}\sigma_r\\ \sigma_\theta\end{Bmatrix}=\left(\begin{bmatrix}m_{11} & 2m_{12}\\ m_{12} & m_{22}\end{bmatrix}\begin{Bmatrix}\frac{du}{dr}\\ \frac{u}{r}\end{Bmatrix}+\begin{Bmatrix}m_{31}\\ m_{32}\end{Bmatrix}T(r)+\begin{Bmatrix}m_{41}\\ m_{42}\end{Bmatrix}C(r)\right)-\begin{Bmatrix}m_{51}\\ m_{52}\end{Bmatrix}\frac{A_1}{r^2} \tag{19}$$

where m_{ij} are functions of r

$$\begin{aligned}&m_{11}=c_{rr}+\frac{(e_{rr})^2}{\varepsilon_{rr}},\ m_{12}=c_{r\theta}+\frac{e_{rr}e_{r\theta}}{\varepsilon_{rr}},\ m_{22}=c_{\theta\varphi}+c_{\theta\theta}+2\frac{(e_{r\theta})^2}{\varepsilon^{rr}}\\ &m_{31}=\frac{e_{rr}p_{11}}{\varepsilon_{rr}}-\lambda_r,\ m_{32}=\frac{e_{r\theta}p_{11}}{\varepsilon_{rr}}-\lambda_\theta,\ m_{41}=-\eta_r\\ &m_{42}=-\eta_\theta,\ m_{51}=\frac{e_{rr}}{\varepsilon_{rr}},\ m_{51}=\frac{e_{r\theta}}{\varepsilon_{rr}}\end{aligned} \tag{20}$$

Therefore, Eq. (7) with the aid of Eq. (19) yields

$$\begin{aligned}&\frac{d^2u}{dr^2}+\left(\frac{2}{r}+\frac{1}{m_{11}}\frac{dm_{11}}{dr}\right)\frac{du}{dr}+2\left(\frac{1}{rm_{11}}\frac{dm_{12}}{dr}+\frac{m_{12}-m_{22}}{r^2m_{11}}\right)u+\frac{m_{41}}{m_{11}}\frac{dC}{dr}\\ &+\left(\frac{1}{m_{11}}\frac{dm_{41}}{dr}+\frac{2(m_{41}-m_{42})}{rm_{11}}\right)C(r)+\frac{m_{31}}{m_{11}}\frac{dT}{dr}+\left(\frac{1}{m_{11}}\frac{dm_{31}}{dr}+\frac{2(m_{31}-m_{32})}{rm_{11}}\right)\end{aligned}$$

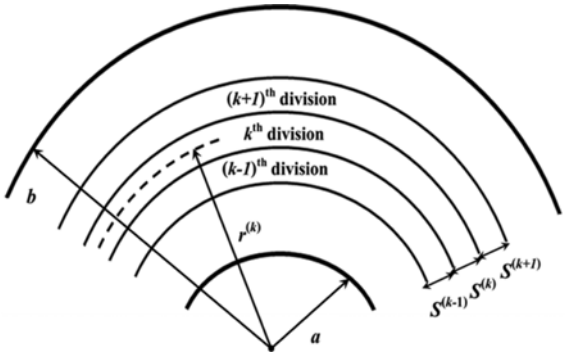

Fig. 2. Dividing Radial Domain Into Some Finite Sub-domain

$$-\left(\frac{1}{r^2m_{11}}\frac{dm_{51}}{dr}-\frac{2m_{52}}{r^3m_{11}}\right)A_1=0 \tag{21}$$

The mechanical boundary conditions of the sphere in question are given by

$$\sigma_r|_{r=a}=-P_1,\quad \sigma_r|_{r=b}=-P_2 \tag{22}$$

where P_1 and P_2 denote the inner and outer pressures, respectively. So, the complete general solution to the radial displacement u may be used to obtain the electric potential. Integrating Eq. (18) gives the electric potential $\psi(r)$ with additional arbitrary integration constant A_2. Finally, the constants A_1 and A_2 are obtained using the electric boundary conditions:

$$\psi(r)|_{r=a}=\psi_1,\quad \psi(r)|_{r=b}=\psi_2 \tag{23}$$

An analytical solution of Eq. (21) with variable coefficients is difficult. Hence, a semi-analytical solution is attempted here (Mendelson, 1968). In this method, the radial domain is divided into several virtual sub-domains with thickness $s^{(k)}$ as shown in Fig. 2. Evaluating the coefficients of Eq. (21) at $r=r^{(k)}$, which is the mean radius of the kth division, and using them instead of the variable coefficients, yields:

$$\frac{d^2u^{(k)}}{dr^2}+N_1^{(k)}\frac{du^{(k)}}{dr}+N_2^{(k)}+u^{(k)}-N_3^{(k)}=0 \tag{24}$$

where

$$\begin{aligned}&N_1^{(k)}=\frac{2}{r^{(k)}}+\frac{1}{m_{11}(r^{(k)})}\frac{dm_{11}}{dr}\bigg|_{r=r^{(k)}}\\ &N_2^{(k)}=\frac{2}{r^{(m)}m_{11}(r^{(k)})}\frac{dm_{12}}{dr}\bigg|_{r=r^{(k)}}+\frac{2[m_{12}(r^{(k)})-m_{22}(r^{(k)})]}{[r^{(k)}]^2m_{11}(r^{(k)})}\\ &N_3^{(k)}=-\frac{m_{41}(r^{(k)})}{m_1(r^{(k)})}\frac{dC}{dr}\bigg|_{r=r^{(k)}}-\frac{m_{31}(r^{(k)})}{m_{11}(r^{(k)})}\frac{dT}{dr}\bigg|_{r=r^{(k)}}\\ &-\frac{1}{m_{11}(r^{(k)})}\left[\frac{dm_{41}}{dr}\bigg|_{r=r^{(k)}}+\frac{2[m_{41}(r^{(k)})-m_{42}(r^{(k)})]}{r^{(k)}}\right]C(r^{(k)})\\ &-\frac{1}{m_{11}(r^{(k)})}\left[\frac{dm_{31}}{dr}\bigg|_{r=r^{(k)}}+\frac{2[m_{31}(r^{(k)})-m_{32}(r^{(k)})]2}{r^{(k)}}\right]T(r^{(k)})\end{aligned}$$

$$+\frac{1}{[r^{(k)}]^2 m_{11}(r^{(k)})}\left[\left.\frac{dm_{51}}{dr}\right|_{r=r^{(k)}}-\frac{2m_{52}(r^{(k)})}{r^{(k)}}\right]A_1^{(k)} \tag{25}$$

Equation (21) with variable coefficients, and using the above technique, is changed into a system of m equations, equal to the number of virtual sub-domains. The solution to Eq. (24) is given by

$$u^{(k)} = B_1^{(k)} e^{\beta_1 r} + B_2^{(k)} e^{\beta_2 r} + \frac{N_3^{(k)}}{N_2^{(k)}} \tag{26}$$

where β_1 and β_2 are the roots of the equation

$\beta^2 + N_1^{(k)}\beta + N_2^{(k)} = 0$, and $B_1^{(k)}$ and $B_2^{(k)}$ are unknown constants for the kth sub-domain. Also, the solution of Eq. (24) is valid for

$$r^{(k)} - \frac{s^{(k)}}{2} \le r \le r^{(k)} + \frac{s^{(k)}}{2} \tag{27}$$

where $s^{(k)}$ and $r^{(k)}$ are the radial width and the mean radius of the kth sub-domain, respectively. The unknowns $B_i^{(k)}$ (i = 1, 2) can be given by applying the necessary conditions between each two adjacent sub-domains. So, the continuities of the radial displacement $u^{(k)}$, the stresses $\sigma_r^{(k)}$ and $\sigma_\theta^{(k)}$, as well as the electric potential $\psi^{(k)}$ are imposed, for this purpose, at the interfaces of the adjacent sub-domains. Then, the interfaces continuity conditions are represented by

$$\Im^{(k)}\Big|_{r=r^{(k)}+\frac{s^{(k)}}{2}} = \Im^{(k+1)}\Big|_{r=r^{(k+1)}-\frac{s^{(k+1)}}{2}} \tag{28}$$

where $\Im$ represents any of the functions u, σ_r, σ_θ, and ψ. The above continuity conditions together with the global boundary conditions given in Eqs. (22) and (23) yields a set of linear algebraic equations in $A_{1,k}$, $A_{2,k}$, $B_{1,k}$, $B_{2,k}$ ($k = 1, 2, \ldots m$). Solving this system of linear algebraic equations and substituting the resulting parameters into Eqs. (26), the displacements $u^{(k)}$ can be determined in each sub-domain. It is to be noted that, increasing the number of sub-domains will improve the accuracy of the numerical results.

4. Numerical Examples and Discussion

Numerical examples for the analysis of FGPM hollow spheres with hygrothermal conditions are given. The material property gradient index n is assumed to take five values: $n = 0$ (outer material), $n = 1$, $n = 2$, $n = 5$, and $n \to \infty$ (inner material). The inner material properties used in the numerical calculations of the FGPM hollow sphere are (Dai *et al.*, 2010a):

$$c_{rr}^a = 1.11\times10^{11}\text{Pa},\ c_{r\theta}^a = 7.78\times10^{10}\text{ Pa},\ c_{\theta z}^a = 1.15\times10^{11}\text{ Pa}$$
$$c_{\theta\theta}^a = 2.2\times10^{11}\text{ Pa}, e_{rr}^a = 15.1\text{ Cm}^{-2}, e_{r\theta}^a = -5.2\text{ Cm}^{-2}$$
$$\varepsilon_{rr}^a = 5.62\times10^{-9}\text{C}^2\text{K}^{-1}\text{m}^2,\ p_{11}^a = -2.5\times10^{-5}\text{Ckm}^{-2}$$
$$\alpha_r^a = 0.0001\text{K}^{-1}, \alpha_\theta^a = 0.00001\text{K}^{-1}$$
$$\eta_r^a = 0.03\times c_{rr}^a,\ \eta_\theta^a = 0 \tag{29}$$

The outer material properties are taken with references to PZT-5 as follows (Ghorbanpour Arani *et al.,* 2011):

$$c_{rr}^b = 1.11\times10^{11}\text{ Pa}, c_{r\theta}^b = 7.52\times10^{10}\text{ Pa},\ c_{\theta z}^b = 7.8\times10^{10}\text{ Pa}$$
$$c_{\theta\theta}^b = 1.2\times10^{11}\text{ Pa}, e_{rr}^b = 15.78\text{ Cm}^{-2}, e_{r\theta}^b = -5.35\text{ Cm}^{-2}$$
$$\varepsilon_{rr}^b = 7.4\times10^{-9}\text{C}^2\text{K}^{-1}\text{m}^2,\ p_{11}^b = -25\times10^{-5}\text{Ckm}^{-2}$$
$$\alpha_r^b = 8.53\times10^{-6}\text{K}^{-1}, \alpha_\theta^b = 1.99\times10^{-6}K^{-1}$$
$$\eta_r^b = 0.03\times c_{rr}^b,\ \ \eta_\theta^b = 0 \tag{30}$$

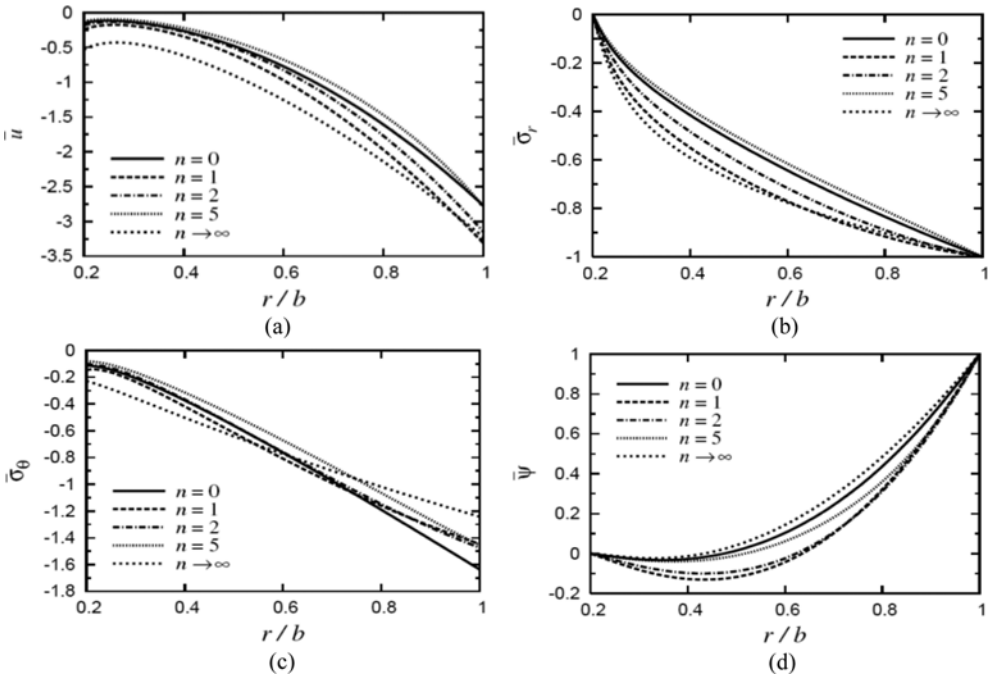

Fig. 3. Field Quantities in the FGPM Hollow Sphere for Different Values of n (Example 1): (a) $\bar{u}$ Versus r/b, (b) $\bar{\sigma}_r$ Versus r/b, (c) $\bar{\sigma}_\theta$ Versus r/b, (d) $\bar{\psi}$ Versus r/b

4.1 Example 1 (mechanical and electrical loads)

The FGPM hollow sphere is subjected to uniform pressure on the external surface and it is traction-free in its internal surface. In addition, the spherical structure is subjected to uniform potential at external surface and it is grounded at the internal surface, that is:

$$P_1 = 0, P_2 = 10^{10} \text{ Pa}, \psi_1 = 0, \psi_2 = 10^8 WA^{-1} \tag{31}$$

Numerical results for such hollow sphere are plotted in Fig. 3. The dimensionless radial displacement, stresses and electric potential are given by

$$\bar{u} = \frac{u}{b}, \ \bar{\sigma}_i = \frac{\sigma_i}{P_2}, \ (i = r, \theta), \ \bar{\psi} = \frac{\psi}{\psi_2} \tag{32}$$

Figure 3(a) shows the distribution of $\bar{u}$ along the radial direction of the FGPM hollow sphere. The radial displacement $\bar{u}$ is no longer increasing and has its maximum near the inner surface of the sphere. The value of $n = 5$ gives the highest displacement while $n \to \infty$ gives the smallest one. Fig. 3(b) shows the radial stress distribution through the radial direction of the FGPM hollow sphere. The radial stress $\bar{\sigma}_r$ for all values of n at $r = a$ is equal to 0 and at $r = b$ is equal to -1, which should be expected in order to satisfy the boundary conditions given in Eq. (22). The differences between radial stresses $\bar{\sigma}_r$ increase near the mid-plane (furthest from internal and external boundaries) of the FGPM hollow sphere. Fig. 3(c) shows the circumferential stress $\bar{\sigma}_\theta$ through the radial direction of the FGPM hollow sphere. It is decreasing to a minimum at the outer surface of the sphere. The value of $n \to \infty$ gives the smallest stress at the inner surface and the greatest stress at the outer surface. However, $n = 0$ gives the smallest stress at the outer surface of the sphere. Fig. 3(d) shows the distribution of the electric potential $\bar{\psi}$ along the radial direction for different values of n of the FGPM hollow sphere. It is to be noted that the electric potential $\bar{\psi}$ at $r = a$ is equal to 0 and at $r = b$ is equal to 1, which satisfies the boundary conditions given in Eq. (22). The differences between electric potentials $\bar{\psi}$ increase near the mid-plane (furthest from internal and external boundaries) of the FGPM hollow sphere. The electric potential $\bar{\psi}$ decreases and has its minimum value near the inner surface of the sphere for $n = 0, 5, \to \infty$ while it has its minimum at $r/b = 0.46$ for $n = 1, 2$. For all n, the electric potential $\bar{\psi}$ increases to maximum values at the outer surface of the sphere.

4.2 Example 2 (mechanical load only)

The FGPM hollow sphere is subjected to uniform internal pressure with free electric potential. This means that the present sphere acts as a sensor. That is:

$$P_1 = 10^{10} \text{ Pa}, P_2 = 0, \psi_1 = \psi_2 = 0 \tag{33}$$

Numerical results for such hollow sphere are plotted in Fig. 4. The dimensionless radial displacement, stresses and electric potential are given by

$$\bar{u} = \frac{u}{b}, \ \bar{\sigma}_i = \frac{\sigma_i}{P_1}, \ (i = r, \theta), \bar{\psi} = \psi \tag{34}$$

Figrue 4 shows the radial displacement, radial and circumferential stresses, and electric potential distributions in the FGPM hollow

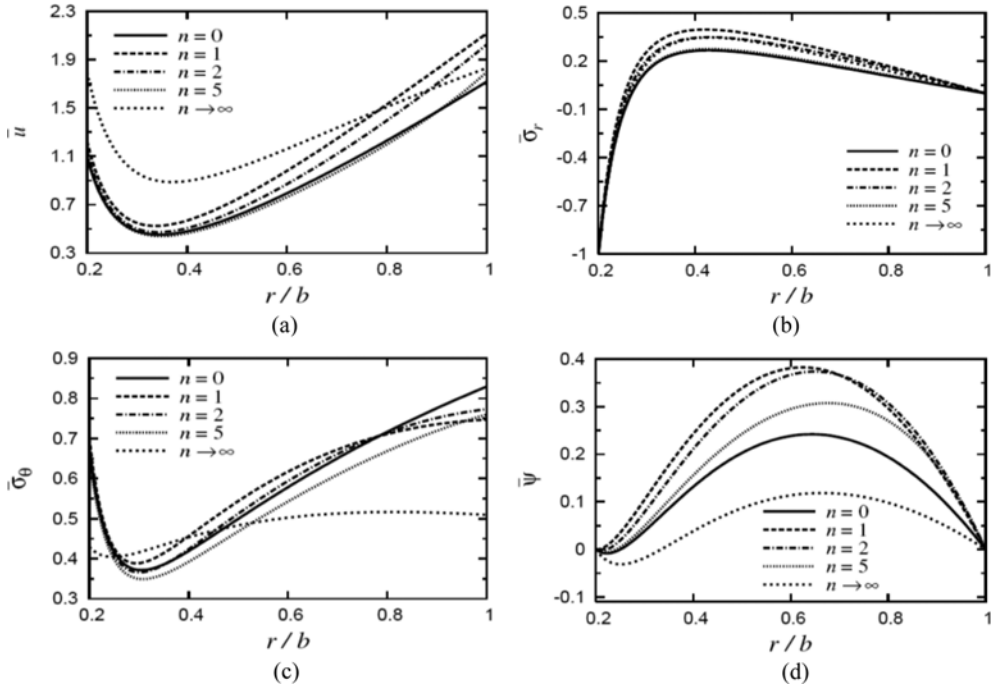

Fig. 4. Field quantities in the FGPM hollow sphere for different values of n (Example 2): (a) $\bar{u}$ Versus *r*/*b*, (b) $\bar{\sigma}_r$ versus *r*/*b*, (c) $\bar{\sigma}_\theta$ Versus *r*/*b*, (d) $\bar{\psi}$ Versus *r*/*b*

sphere. Fig. 4(a) shows that the radial displacement $\bar{u}$ is no longer decreasing and has its minimum value at $r/b = 0.35$ for different n. Fig. 4(b) shows that the radial stress $\bar{\sigma}_r$ for different values of n at $r = a$ is equal to -1 and at $r = b$ is equal to 0, which should be expected in order to satisfy the boundary conditions given in Eq. (22). The differences between radial stresses $\bar{\sigma}_r$ increase at $r/b = 0.4$ in which the maximum value of $\bar{\sigma}_r$ occurs. Fig. 4(c) shows that the circumferential stress $\bar{\sigma}_\theta$ decreases to its minimum value at $r/b = 0.23$ for $n \to \infty$ and at $r/b = 0.31$ for other values of n. Fig. 4d shows that the electric potential $\bar{\psi}$ vanishes at $r = as$ and at $r = b$, which should be expected in order to satisfy the boundary conditions. The differences between electric potentials $\bar{\psi}$ increase near the mid-plane of the FGPM hollow sphere. The maximum value of the electric potential $\bar{\psi}$ occurs at different positions according to the value of n.

4.3 Example 3 (electrical load only):

The hollow sphere is considered with traction free and it is subjected to a constant voltage at internal surface and grounded at the external surface. In this case, the sphere acts as an actuator, that is:

$$P_1 = P_2 = 0,\ \psi_1 = 10^8 WA^{-1},\ \psi_2 = 0 \tag{35}$$

The dimensionless radial displacement, stresses and electric potential are given by

$$\bar{u} = \frac{u}{b},\ \bar{\sigma}_i = \sigma_i,\ \ (i = r, \theta),\ \bar{\psi} = \frac{\psi}{\psi_1} \tag{36}$$

Figure 5 shows the plots of the field quantities versus the radial directions of the FGPM hollow sphere. Fig. 5(a) shows that the radial displacement $\bar{u}$ is no longer decreasing and has its minimum value at $r/b = 0.27$ for different n. Fig. 5(b) shows that the radial stress $\bar{\sigma}_r$ is equal to 0 at $r = a$ and $r = b$ for different values of n, which should be expected in order to satisfy the boundary conditions. The differences between radial stresses $\bar{\sigma}_r$ increase at $r/b = 0.33$ in which the maximum value of $\bar{\sigma}_r$ occurs. At this position, $n \to \infty$ gives the greatest radial stress while $n = 5$ gives the smallest one. Fig. 5(c) shows that the circumferential stress $\bar{\sigma}_\theta$ is decreasing to get its minimum near the inner surface of the FGPM hollow sphere. After that, it is increasing to get its maximum at the outer surface. This is done for all values of n except $n \to \infty$ for which $\bar{\sigma}_\theta$ increases directly from the inner to the outer surfaces of the sphere. Fig. 5(d) shows that the electric potential $\bar{\psi}$ vanishes at $r = b$ and is equal to 1 at $r = a$, which satisfies fully the boundary conditions. The differences between electric potentials $\bar{\psi}$ increase at $r/b = 0.5$. The maximum value of the electric potential $\bar{\psi}$ occurs at different neighborhood positions according to the value of n. For $n \to \infty$, $\bar{\psi}$ is maximum at the inner surface of the sphere.

4.4 Example 4 (free of mechanical and electrical loads)

The hollow sphere is considered with traction and electrical load free, that is:

$$P_1 = P_2 = 0,\ \ \psi_1 = \psi_2 = 0 \tag{37}$$

Numerical results for such hollow sphere are plotted in Fig. 6. The dimensionless radial displacement, stresses and electric

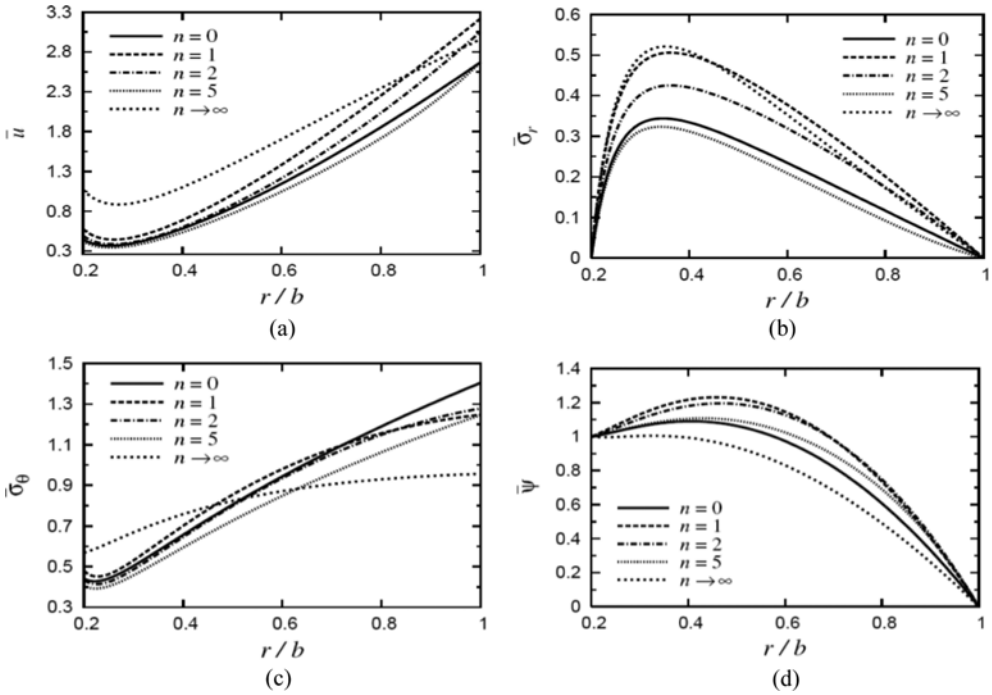

Fig. 5. Field Quantities in the FGPM Hollow Sphere for Different Values of n (Example 3): (a) $\bar{u}$ Versus r/b, (b) $\bar{\sigma}_r$ Versus r/b, (c) $\bar{\sigma}_\theta$ Versus r/b, (d) $\bar{\psi}$ versus r/b

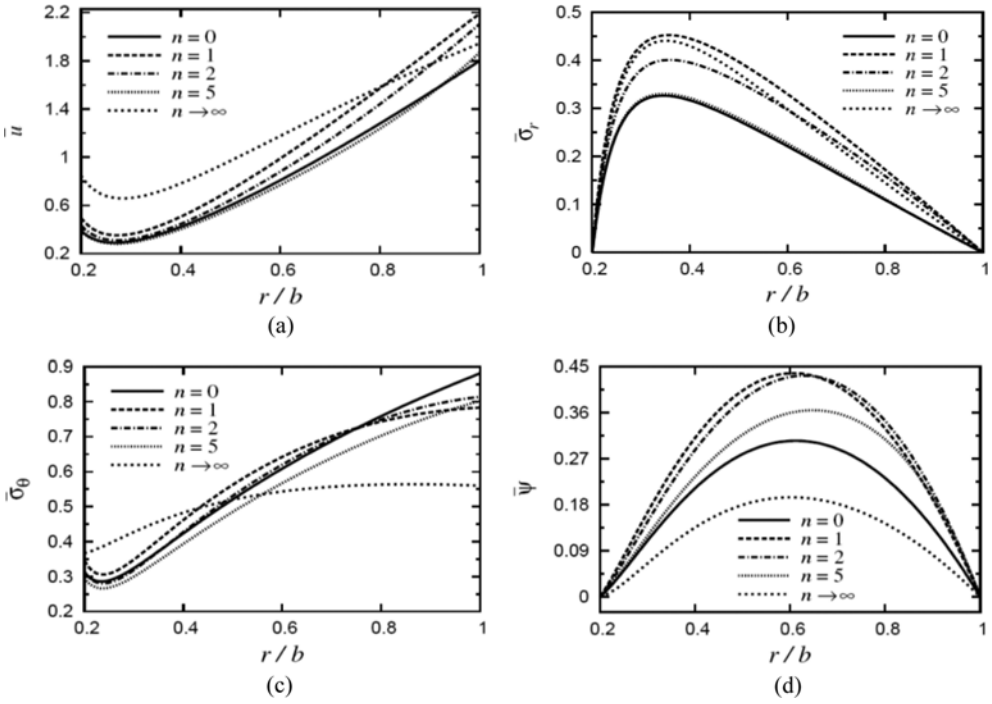

Fig. 6. Field Quantities in the FGPM Hollow Sphere for Different Values of *n* (Example 4): (a) $\bar{u}$ versus *r*/*b*, (b) $\bar{\sigma}_r$ Versus *r*/*b*, (c) $\bar{\sigma}_\theta$ Versus *r*/*b*, (d) $\bar{\psi}$ Versus *r*/*b*

potential are given by

$$\bar{u} = \frac{u}{b},\ \bar{\sigma}_i = \sigma_i,\ (i = r, \theta),\ \ \bar{\psi} = \psi \tag{38}$$

Figure 6(a) shows that the radial displacement $\bar{u}$ decreases to its minimum value at the same position ($r/b = 0.3$) for different *n*. The maximum values of $\bar{u}$ occur at the external surface of the sphere. Fig. 6(b) shows that the radial stress $\bar{\sigma}_r$ is equal to 0 at $r = a$ and $r = b$ for different values of *n* as mentioned before. It has the same behavior as that in Fig. 5(b). However, $n = 1$ gives the greatest radial stress while $n = 0$ gives the smallest one. Also, Fig. 6(c) shows that the circumferential stress $\bar{\sigma}_\theta$ has the same behavior as that in Fig. 5(c). Fig. 6(d) shows that the electric potential $\bar{\psi}$ vanishes at $r = a$ and $r = b$ as mentioned before. The differences between electric potentials $\bar{\psi}$ increase at $r/b = 0.6$. The maximum values of $\bar{\psi}$ occur at different neighborhood positions according to the value of *n*.

5. Conclusions

The hygrothermal analysis of a functionally graded piezoelectric hollow sphere is investigated in this paper. A semi-analytical solution technique is developed for the electro-thermo-hygro-mechanical problem, where stresses and electric potentials are produced under combined mechanical and electrical loading conditions. It is to be noted that the gradation of the constitutive components plays an important role to control the distribution of stresses, radial displacement, and electric potential responses of FGPM as well as in optimal design of this structure. Thus by selecting a proper value of the grading index *n* and suitable loads, it is possible for engineers to design a FGPM hollow sphere that can meet specific requirements. Finally, it is concluded from the above analyses and discussion that the presented method is simple and effective and the semi-analytical solution is accurate (within the context of numerical analyses) and reliable.

References

Allam, M. N. M. and Tantawy, R. (2011). "Thermomagnetic viscoelastic responses in functionally graded hollow structures." *Acta Mech. Sin.,* Vol. 27, No. 4, pp. 567-577, DOI: 10.1007/s10409-011-0467-3.

Bahrami, A. and Nasier, A. (2007). "Interlaminar hygrothermal stresses in laminated plates." *Int. J. Solids Struct.*, Vol. 44, Nos. 25-26, pp. 8119-8142, DOI: 10.1016/j.ijsolstr.2007.06.004.

Dai, H.-L. and Wang, X. (2005). "Thermo-electro-elastic transient responses in piezoelectric hollow structures." *Int. J. Solids Struct.*, Vol. 42, Nos. 3-4, pp. 1151-1171, DOI: 10.1016/j.ijsolstr.2004.06.061.

Dai, H.-L., Fu, Y. M., and Yang, J. H. (2007). "Electromagnetoelastic behaviors of functionally graded piezoelectric solid cylinder and sphere." *Acta Mech. Sin.*, Vol. 23, No. 1, pp. 55-63, DOI: 10.1007/s10409-006-0047-0.

Dai, H.-L., Hong, L., Fu, Y. M., and Xiao, X. (2010a). "Analytical solution for electromagnetothermoelastic behaviors of a functionally graded piezoelectric hollow cylinder." *Appl. Math. Model.*, Vol. 34, No. 2, pp. 343-357, DOI: 10.1016/j.apm.2009.04.008.

Dai, H.-L., Jiang, H. J., and Yang, L. (2012). "Time-dependent behaviors of a FGPM hollow sphere under the coupling of multi-fields." *Solid State Sci.*, Vol. 14, No. 5, pp. 587-597, DPI: 10.1016/j.solidstatesciences.2012.02.011.

Dai, H.-L., Xiao, X., and Fu, Y. M. (2010b). "Analytical solutions of stresses in functionally graded piezoelectric hollow structures." *Solid State Commun.*, Vol. 150, Nos. 15-16, pp. 763-767, DOI: 10.1016/j.ssc.2010.01.028.

Ghorbanpour Arani, A., Kolahchi, R., and Mosallaie Barzoki, A. A. (2011). "Effect of material in-homogeneity on electro-thermo-mechanical behaviors of functionally graded piezoelectric rotating shaft." *Appl. Math. Model.*, Vol. 35, No. 6, pp. 2771-2789, DOI: 10.1016/j.apm.2010.11.076.

Heyliger, P. (1997). "A note on the static behavior of simply-supported laminated piezoelectric cylinders." *Int. J. Solids Struct.*, Vol. 34, No. 29, pp. 3781-3794, DOI: 10.1016/S0020-7683(97)00009-7.

Lo, S. H., Zhen, W. U., Cheung, Y. K., and Wanji, C. (2010). "Hygrothermal effects on multilayered composite plates using a refined higher order theory." *Compos. Struct.*, Vol. 92, No. 3, pp. 633-646, DOI: 10.1016/j.compstruct.2009.09.034.

Loghman, A., Aleayoub, S. M. A., and Hasani Sadi, M. (2012). "Time-dependent magnetothermoelastic creep modeling of FGM spheres using method of successive elastic solution." *Appl. Math. Model.*, Vol. 36, No. 2, pp. 836-845, DOI: 10.1016/j.apm.2011.07.038.

Mendelson, A. (1968). *Plasticity Theory and Applications*, Macmillan, New York.

Ootao, Y. and Tanigawa, Y. (2007). "Transient piezothermoelastic analysis for a functionally graded thermopiezoelectric hollow sphere." *Compos. Struct.*, Vol. 81, No. 4, pp. 540-549, DOI: 10.1016/j.compstruct.2006.10.002.

Patel, B. P., GanaPathi, M., and Makhecha, D. P. (2002). "Hygrothermal effect on the structural behavior of thick composite laminates using higher-order theory." *Compos. Struct.*, Vol. 56, No. 1, pp. 25-34, DOI: 10.1016/S0263-8223(01)00182-9.

Raja, S., Sinha, P. K., Prathap, G., and Dwarakanathan, D. (2004). "Influence of active stiffening on dynamic behavior of piezo-hygro-thermo elastic composite plates and shell." *J. Sound Vib.*, Vol. 278, Nos. 1-2, pp. 257-283, DOI: 10.1016/j.jsv.2003.10.002.

Reddy, J. N. (2000). "Analysis of functionally graded plates", *Int. J. Numer. Meth. Eng.*, Vol. 47, Nos. 1-3, pp. 663-684, DOI: 10.1002/(SICI)1097-0207.

Reddy, J. N. and Cheng, Z. Q. (2001). "Three-dimensional thermomechanical deformations of functionally graded rectangular plates." *Eur. J. Mech. - A/Solids*, Vol. 20, No. 5, pp. 841-855, DOI: 10.1016/S0997-7538(01)01174-3.

Reddy, J. N. and Chin, C. D. (1998). "Thermomechanical analysis of functionally graded cylinders and plates." *J. Therm. Stresses*, Vol. 21, No. 6, pp. 593-626, DOI: 10.1080/01495739808956165.

Sinha, D. K. (1962). "Note on the radial deformation of a piezoelectric polarized spherical shell with symmetrical temperature distribution." *J. Acoust. Soc. Am.*, Vol. 34, No. 8, pp. 1073-1075, DOI: 10.1121/1.1918247.

Whiteny, J. M. and Ashton, J. E. (1971). "Effect of environment on the elastic response of layered composite plates." *AIAA J.*, Vol. 9, No. 9, pp. 1708-1713, DOI: 10.2514/3.49976.

Zenkour, A. M. (2005a). "A comprehensive analysis of functionally graded sandwich plates: Part 1 Deflection and stresses." *Int. J. Solids Struct.*, Vol. 42, Nos. 18-19, pp. 5224-5242, DOI: 10.1016/j.ijsolstr.2005.02.015.

Zenkour, A. M. (2005b). "A comprehensive analysis of functionally graded sandwich plates: Part 2 Buckling and free vibration." *Int. J. Solids Struct.*, Vol. 42, Nos. 18-19, pp. 5243-5258, DOI: 10.1016/j.ijsolstr.2005.02.016.

Zenkour, A. M. (2006a). "Generalized shear deformation theory for bending analysis of functionally graded plates." *Appl. Math. Model.*, Vol. 30, No. 1, pp. 67-84, DOI: 10.1016/j.apm.2005.03.009.

Zenkour, A. M. (2006b) "Steady-state thermoelastic analysis of a functionally graded rotating annular disk." *Int. J. Struct. Stab. Dyna.*, Vol. 6, No. 4, pp. 1-16, DOI: 10.1142/S0219455406002064.

Zenkour, A. M. (2007) "Benchmark trigonometric and 3-D elasticity solutions for an exponentially graded thick rectangular plate." *Arch. Appl. Mech.*, Vol. 77, No. 4, pp. 197-214, DOI: 10.1007/s00419-006-0084-y.

Zenkour, A. M. (2012a). "Hygrothermal analysis of exponentially graded rectangular plates." *J. Mech. Mater. Struct.*, Vol. 7, No. 7, pp. 687-700, DOI: 10.2140/jomms.2012.7.687.

Zenkour, A. M. (2012b). "Hygrothermal effects on the bending of angle-ply composite plates using a sinusoidal theory." *Compos. Struct.*, Vol. 94, No. 12, pp. 3685-3696, DOI: 10.1016/j.compstruct.2012.05.033.

Zenkour, A. M., Elsibai, K. A., and Mashat, D. S. (2008). "Elastic and viscoelastic solutions to rotating functionally graded hollow and solid cylinders." *Appl. Math. Mech.* (*English Ed.*), Vol. 29, No. 12, pp. 1601-1616, DOI: 10.1007/s10483-008-1208-x.